# ORIGINAL ARTICLE

# Influence of respiratory motion correction on quantification of myocardial perfusion SPECT

Ahmad Bitarafan-Rajabi, PhD,[a] Hossein Rajabi, MD,[b] Feridoon Rastgou, MD,[a]
Hasan Firoozabady, MD,[a] Nahid Yaghoobi, MD,[a] Hadi Malek, MD,[a]
Werner Langesteger, MD,[c] and Mohsen Beheshti, MD[c]

[a] Department of Nuclear Medicine, Rajaie Cardiovasular, Medical & Research Center, Iran University of Medical Sciences, Tehran, Iran
[b] Department of Medical Physics, School of Medical Sciences, Tarbiat Modares University, Tehran, Iran
[c] Department of Nuclear Medicine & Endocrinology, St Vincent's Hospital, PET - CT Center Linz, Linz, Austria

*Background.* Respiratory-related cardiac motion could have considerable effects on myocardial perfusion imaging, leading to misinterpretation of the images. In this study, we examined the influence of respiratory correction on ECG-gated myocardial perfusion SPECT (RC-GSPECT) concerning regional myocardial perfusion and function.

*Materials and Methods.* Using the NCAT phantom, a typical torso phantom was generated. SimSET, a Monte Carlo simulator, was used to image the photon emerging from the phantom. Twenty-six patients underwent a 2-day stress-rest ECG-gated myocardial perfusion SPECT (GSPECT) imaging. A separate study was also performed by simultaneous respiratory and cardiac triggering with the real-time position management (RPM) for respiratory correction (RC).

*Results.* In simulation study, count density in the inferior and inferoseptal walls increased in the lower bin of the respiratory cycle. On the other hand, there was a higher correlation between RC-GSPECT and echocardiography for left ventricular ejection fraction (LVEF) ($r = 0.95$, $P < .01$ vs $r = 0.88$, $P < .01$ for GSPECT).

*Conclusion.* We proposed a new approach for respiratory and cardiac-gated SPECT to eliminate respiratory motion artifacts. RC-GSPECT is a feasible method in MPI studies and may play an important role to improve the quality of MPI images, particularly in the inferior wall. (J Nucl Cardiol 2015;22:1019–30.)

Key Words: $^{99m}$Tc-tetrofosmin · myocardial perfusion · gated SPECT · respiratory correction

## INTRODUCTION

$^{99m}$Tc-based myocardial-gated SPECT has been established as an important diagnostic and prognostic method for the assessment of patients with coronary artery disease (CAD).[1,2] Respiratory motion, nevertheless, is supposed to be one of the influential factors on the quality of the images and may lead to the misinterpretation of ECG-gated myocardial perfusion SPECT (GSPECT) studies.[3,4] Respiration entails the motion of the diaphragm, heart, thorax, lungs, liver, and spleen.[5] In humans, diaphragm and consequently heart motions have been estimated to be about 1.5 cm during a tidal breathing.[6] Deeper breathing increases the amplitude of the diaphragm movement and may produce image artifacts, depending on the concentration and distribution of the sub-diaphragmatic activity.[7]

The adverse effect of the respiratory motion on the interpretation of ECG-gated SPECT, computed

tomography (CT), and magnetic resonance imaging (MRI) as well as positron emission tomography (PET) has been shown in some studies,[8-11] and several techniques have been introduced to overcome this limitation in different imaging modalities.[12-15] In simulation studies, the adverse effects of respiratory motion in cardiac SPECT-reconstructed images have been shown.[12,14] However, there is not yet a full knowledge of the respiratory motion on the quantitative clinical parameters derived from GSPECT. Some respiratory-induced motion artifacts can be corrected by dedicated software, depending on the pattern of movement.[16]

On the other hand, different instruments have been used for the amplitude assessment of respiratory motion and respiratory correction (RC). Commonly, a pneumatic bellow is placed around the mid-abdomen of the patient.[17] Livieratos et al[18] used an inductive respiration monitor with a belt around the patient's chest. Also, Beach et al[17] used the Polaris system during cardiac imaging. Recently, the real-time position management (RPM) respiratory gating system (Varian Medical Systems) was introduced to minimize the effect of respiratory motion in different imaging modalities.[13]

In this study, we performed both simulation and clinical studies. In the simulation study, we used a realistic phantom to model both cardiac and respiratory motions. Simulation System for Emission Tomography (SimSET) simulator was used to make the GSPECT images of the phantoms.

In the clinical study, we focused on the implementation and performance of RC on ECG-gated myocardial perfusion SPECT (RC-GSPECT), utilizing the RPM system for respiratory motion correction in GSPECT.

## MATERIALS AND METHODS

### Simulation Study

Using the NURBS-based Cardiac-Torso (NCAT) phantom, a typical torso phantom was generated. The NCAT Phantom was used to imitate the anatomical variations during the cardiac and respiratory cycles. We assumed a cardiac cycle of 0.8 second and respiratory cycle of 5 seconds. The amplitude of respiration was 15 mm. Activity concentration ratios in the lung, body, liver, and LV were 1, 2, 8, and 15, respectively. In order to have a GSPECT study of 8 frames per second, 1,600 pairs of the phantoms (attenuation map and activity distribution) were generated. Phantoms were constructed in 256 * 256 * 256 matrix size. The attenuation coefficients of the tissues in the phantoms were translated into Zubal phantom attenuation indexes in order to feed the Monte Carlo simulator.

SimSET, a Monte Carlo simulator, was used to image the photon emerging from the phantoms.

The parameters and the dimensions of the simulator were adjusted according to the GE SPECT system specification (DST XLi Sopha system) equipped with the low-energy high-resolution collimator. The LEHR collimator had a parallel-hole thickness of 3.5 mm, hole radius of 0.08 mm, and septa thickness of 0.016 mm. Imaging was performed in supine position, and 32 projections of 64 × 64 matrix size (pixel size = 4.8 at zoom factor of 1.33) were acquired over 180° from right anterior oblique to left anterior oblique as per the cardiac-gated protocol. The energy resolution of the system was assumed to be 9.7%, and the counts were collected in the range of 126-154 keV (140 ± %10 keV energy windows). The data simulated a 160-second imaging cycle with 1,600 time-frames, 0.1 second each. Gating was performed as 8 frames per cycle and the data were saved in Interfile format.

Image reconstruction and processing by the ordered-subset expectation maximization (OSEM) method were performed with an interview XP (version 1.04.026 build 41) without any attenuation or scatter correction. Emory cardiac toolbox (ECTb) software (version 3.0, Emory University) was used for the visual and quantitative analysis of the LV regional perfusion. The regional perfusion was measured according to a 13-segment polar map. The model uses three short-axis portions (apical, mid-ventricular, and basal) divided into four segments of anterior, lateral, inferior, and septal segments for each portion and one vertical long-axis slice to represent the LV apex. All reconstructed images were interpreted both visually and quantitatively by two experienced nuclear physicians.

The respiratory correction RC was done based on the simulation study. Therefore, respiratory motion amplitude was defined to three bins: upper, middle, and lower of the respiratory cycle. ECG cycles were selected according to the lower bin, summation of the upper and middle bins, and the total bin, as is illustrated in Figure 1.

### Clinical Study

**Patient.** In this study, 26 (11 males and 15 females; ages 65.2 ± 9.9 years from 46 to 79) known or suspected cases of CAD were examined. Twenty-three patients underwent both the pharmacological stress and the rest studies. Two patients performed the rest study and one patient underwent the pharmacological stress study only. All patients with a history of pulmonary disease, dyspnea, arrhythmia, and left bundle branch block (LBBB) as well as all of the images containing significant extracardiac activity or motion artifacts related to the patient's body movement were excluded from our study. Based on clinical and scintigraphic findings, 14 out of 26 patients underwent selective coronary angiography (SCA) and all the patients had echocardiography within ±1 week of the test. According to the SCA, three patients had normal coronary arteries and 11 patients demonstrated significant coronary vessel disease (VD), i.e., >70% stenosis, comprising four patients with single VD, four patients with two VD, and three patients with three VD. Of all these patients, three had significant and four had non-significant stenosis in the left anterior descending (LAD) artery, three patients had significant and five had non-significant stenosis in the right coronary artery (RCA), and seven had significant stenosis in the left circumflex artery (LCX) as well. Local Ethics Committee
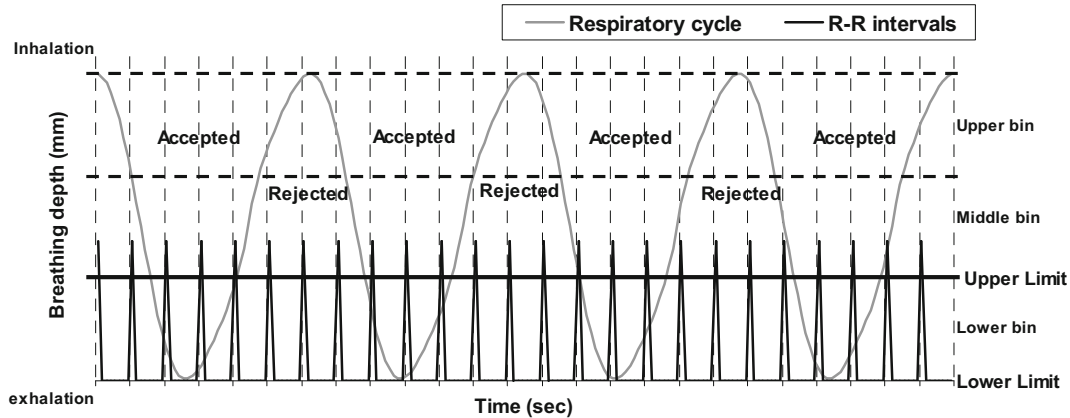
**Figure 1.** Rejected and accepted cardiac cycles in simulation study based on respiratory correction in clinical study.

approved this study. All the patients gave their informed consents.

**ECG-gated acquisition.** Two-day stress-rest imaging protocol was performed with intravenous injection of 740 MBq $^{99m}$Tc-tetrofosmin in each phase of the study. Imaging was performed 45 minutes after radiotracer injection in the GSPECT and subsequently in RC-GSPECT method. All acquisitions were performed by a dual-head variable angle gamma camera (DST XLi Sopha system) equipped with parallel-hole low-energy high resolution (LEHR) collimators. For each study, thirty-two 50-second projections were acquired with $64 \times 64$ matrix size and 1.33 zoom factor (pixel size = 0.66 cm) in an elliptical orbit of 180° (45° RAO-to-LPO) in step and shoot mode. Gating was performed as 8 frames per cycle. The acceptance window for R-R interval was set to 80% in order to acquire all of the acceptable RC cardiac cycles.

## Equipments

Respiratory signals were recorded by a CT-RPM$^{TM}$ interface (Varian Medical System, Palo Alto, California USA), consisting of a marker block, an infrared illuminator ring, a charge-coupled device (CCD) tracking camera, a viewfinder, and RPM software (version 1.6) that displayed and recorded the respiratory motion signals. Reflective external marker was placed on the patient's abdominal surface, at the midpoint between the xiphoid process and the umbilicus (Figure 2). Respiratory signals were recorded by the tracking infrared illuminator/CCD camera. The motion signal was displayed as a graphical waveform on the RPM workstation, representing the patient's respiratory pattern as a function of time. The inspiration and expiration periods were estimated separately by the RPM. The waveform indicated the extent of the motion of the reflective marker on the millimeter scale. We put minimum and maximum thresholds for the amplitude of the respiratory motion signal to control the cardiac signal transmission.



**Figure 2.** The respiratory gating equipment mounted on the SPECT system. The RPM system, an infrared reflective plastic box, is placed on the patient's abdominal surface and the camera with an infrared illuminator surrounding the lens is placed on the SPECT bed.

## Respiratory Correction (RC)

RC was done based on patient's respiratory motions, and respiratory gating was defined according to the breath amplitude. The patients were monitored for a period of 1-3 minutes to achieve the baseline respiratory pattern by the RPM system. The RPM system recorded phase, amplitude (inspiration and expiration amplitudes), and periods within a respiratory cycle. The end-inspiration and the end-expiration were calculated for ten consecutive respiration cycles for each patient. When the amplitude of the respiratory cycle was out of the acceptable borders, the cardiac signal was blocked; otherwise, it was transmitted to the acquisition system (Figure 3). This threshold was compatible with the beginning of inspiration and the end of expiration.
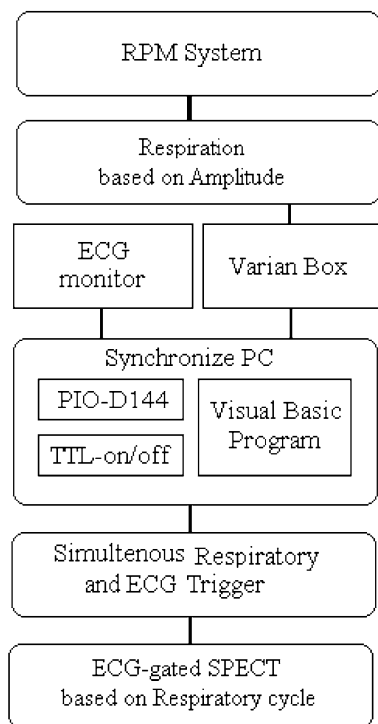
**Figure 3.** The RC-GSPECT diagram, the ECG monitor, and the RPM camera were connected to the synchronization computer and the output of this computer was set up for connection to the gamma camera. The PIO-D144 (ICP DAS Co.), which is transistor-transistor logic (TTL) compatible, was used as an input interface for simultaneous detection of both ECG and respiration signals. The ECG and respiratory cycles were detected by the TTL program on the PIO-D144 input to control the output of ECG cycles according to the respiratory cycles.

## Data Processing

Image reconstruction and processing were performed on a Xeleris workstation (GE software version 1.0 M4). Data were reconstructed using the ordered subsets exceptional maximization (OSEM) method without attenuation and scatter correction. 4D-MSPECT software (revision 1, University of Michigan) was used for the quantitative analysis of the LV regional myocardial perfusion and function. The regional perfusion was measured according to a 20-segment polar map. The perfusion polar map is normalized to peak activity by finding the maximum regional activity in the region's basal and distal rings. The LV perfusion was analyzed because of seven walls, consisting of the anterior, inferior, anteroseptal, inferoseptal, anterolateral, and inferolateral walls as well as the apex.

All the data were correlated with the echocardiographic results. All the echocardiograms were performed in the left lateral decubitus position with apical two- and four-chamber views, and end-diastole volume (EDV), end-systole volume (ESV), and ejection fraction (EF) were measured, using the biplane Simpson's rule by an expert echocardiographer, blinded to the results of the gated SPECT.

## Patient Interpretation

All the GSPECT and RC-GSPECT reconstructed images were interpreted visually, semi-quantitatively, and quantitatively by two experienced nuclear physicians without any access to clinical data such as SCA and echocardiography. In semi-quantitative interpretation of the SPECT perfusion images, the severity of each segmental perfusion defect was rated on a 5-point scale: 0, normal; 1, equivocal; 2, moderately decreased uptake; 3, severely decreased uptake; and 4, no uptake. These scores were assigned for both stress and rest images. A segmental score of 2 or greater was assigned to be abnormal on both the GSPECT and RC-GSPECT. The summed stress score (SSS), summed rest score (SRS), and summed difference score (SDS) were then calculated.

## Statistic

All the data are presented as mean ± standard deviation (SD). The results of the GSPECT and RC-GSPECT were compared using the paired $t$ test with $P$ value <.05. Pearson's correlation was used to assess the correlation between the parameters derived with GSPECT and RC-GSPECT and those with echocardiography. The agreement between the methods was evaluated using the Bland-Altman analysis.[19] All of the statistical data were analyzed by SPSS software package (SPSS Inc., Chicago, IL, USA).

## RESULTS

### Simulation Study

In this section, we present results obtained from the simulation study using the SimSET. For the respiratory correction, the following were considered: (1) lower bin; (2) summation of upper and middle bins; and (3) total bin (Figure 1).

Figure 4 illustrates the polar maps and the short-axis slices obtained by the simulation study at (A) total bin, (B) summation of upper and middle bins, and (C) lower bin of the respiratory cycle. Count density in the inferior and inferoseptal walls increased in the lower bin of the respiratory cycle compared to the total bin as well as the summation of the upper and middle bins. Our results showed that the mean differences of the maximal percentage uptake between the lower bin and total bin in the inferior, anteroseptal, inferoseptal walls were 11.24%, 4.34%, and 5.95%, respectively and the mean difference of the percentage uptake in the total walls was 4.46%. Furthermore, the mean differences of the maximal percentage uptake between the lower bin and the summation of the upper and middle bins in the inferior, anteroseptal, and inferoseptal walls were 15.12%, 3.45%, and 8.34%, respectively, and the mean difference of the percentage uptake in the total walls was 5.23%.
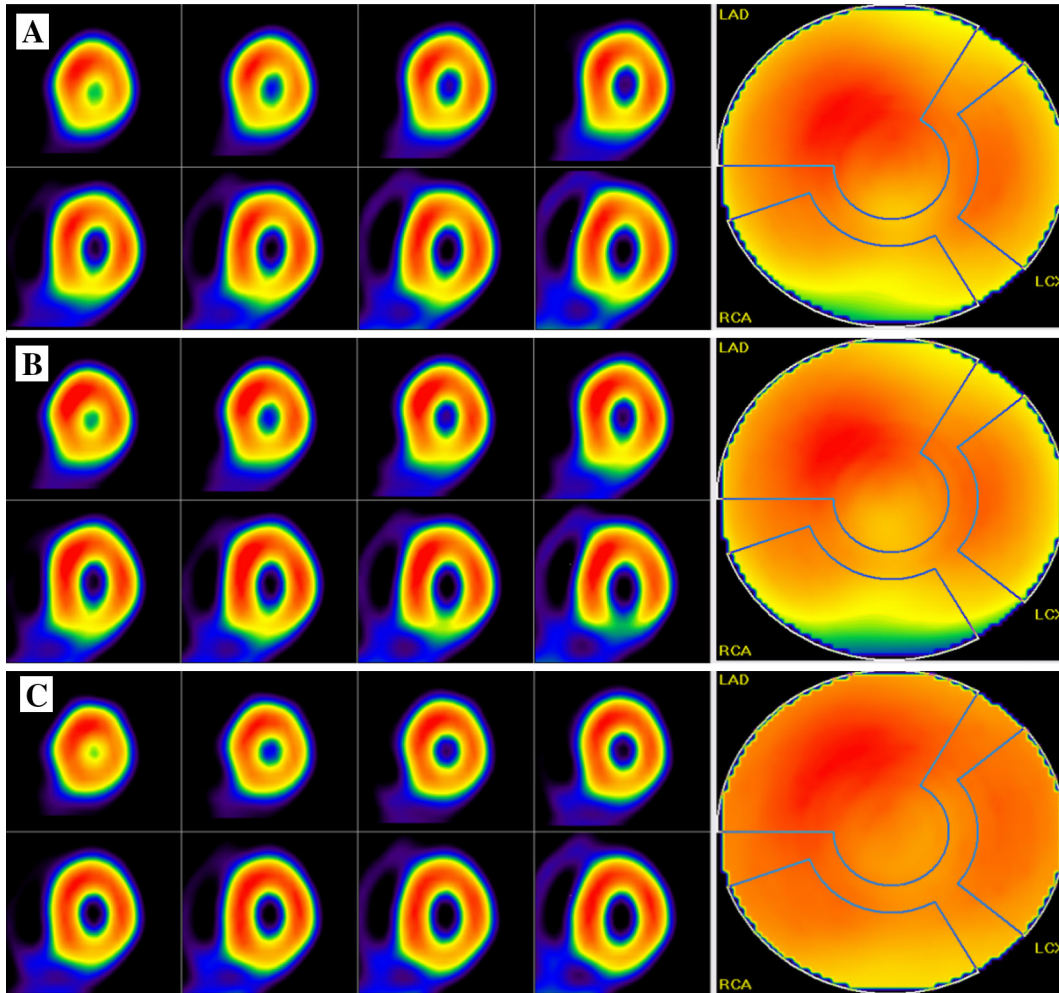
**Figure 4.** Results (polar maps and short-axis slices) obtained by simulation study (**A**) total bins, (**B**) summation of upper and middle bin, and (**C**) lower bin of respiratory cycle. Count density in the inferior and inferoseptal walls increased in lower bin of respiratory cycle compared to total bins as well as summation of upper and middle potion.

To quantify these observations, we plotted the count density percentage vs the LV segments with the accepted and rejected ECG cycles as well as all the ECG cycles by the simulation study in Figure 5. The best presentation was achieved in the lower bin of the respiratory cycle for respiratory correction.

## Clinical Study

In our patients, the respiratory period in the stress phase was 15% shorter than that in the rest phase. This reduction was 10% and 20% for the inspiration and expiration phases, respectively (Figure 6). The respiratory movement of the thoracic wall in the superior-inferior direction was 8.8-16.6 mm (12.4 ± 2.9) and 7.8-11.8 mm (9.5 ± 1.6) for the stress and rest MPI, respectively.

Nineteen out of the twenty-six patients (73.1%) showed abnormal myocardial perfusion scan; these 19 patients consisted of 9 (47.4%) females and 10 (52.6%) males. On the other hand, among the 15 female patients, 9 (60%) had abnormal and 6 (40%) had normal studies and among the 11 male patients, 10 (90.9%) showed perfusion defects and 1 (9.1%) revealed a normal study. Of the 9 positive female patients, 9 (90.9%) cases showed multiple perfusion defects and 1 (11.1%) case revealed single localized perfusion abnormality. Of the 10 males with positive scan, 3 (30%) cases revealed single and 7 (70%) cases demonstrated multiple perfusion defects. The defects were localized in the LAD territory in 22, the RCA territory in 11, and in the LCX territory in 10 cases. It must be noted that all the perfusion defects were reversible and there was no significant difference in visual diagnosis between the

two methods. All demographic data is depicted in Table 1.

The patient population was divided into two groups: one with SCA (Group 1) and the other without SCA (Group 2). In Group 2, the mean percentage of count density in RC-GSPECT was significantly higher than GSPECT in the inferior wall (79% ± 13.1% vs 73% ± 13.3%, respectively; $P < .001$) despite insignificant difference in the segmental visual assessment
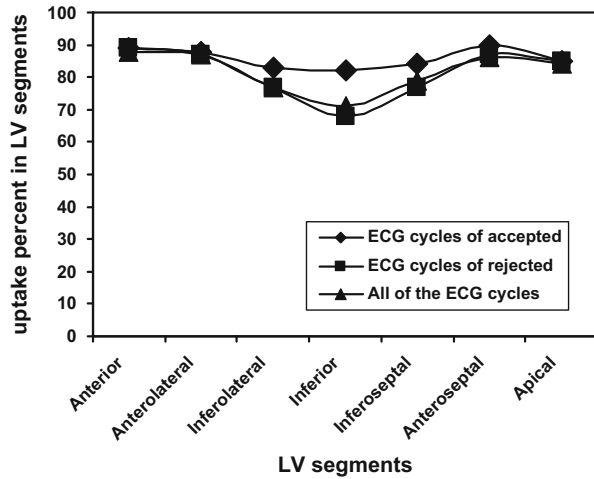


**Figure 5.** The count density percentage vs left ventricular segments with the accepted and rejected ECG cycles as well as all the ECG cycles computed for images obtained by simulation study.

between these two methods (Table 2). In Group 1, however, the mean percentage of count density of the inferior, anteroseptal, and inferoseptal walls in RC-GSPECT was significantly higher than GSPECT ($P < .001$), while in the anterior, anterolateral, inferolateral, and apical walls it was insignificant (Table 2). On the other hand, fourteen patients had concordant results with SCA and RC-GSPECT vs 12 concordant results between SCA and GSPECT. Two patients who had discordant results in the latter group were obese females with ischemia, especially in the inferior wall. Both patients were obese females 87 and 85 kg in weight and 163 and 155 cm in height (body mass index (BMI); 32.7 and 35.4), respectively. There was one patient whose GSPECT was interpreted as ischemia in the mid anterior, mid inferior, anteroapical, and inferoapical segments (SSS = 4, SRS = 11, SDS = 7) vs RC-GSPECT (SSS = 6, SRS = 10, SDS = 4) concordant SCA. Another patient, whose GSPECT was interpreted as mild ischemia in the basal anterolateral and basal inferolateral segments as well as the apex (SSS = 6, SRS = 4, SDS = 2) vs RC-GSPECT (SSS = 6, SRS = 3, SDS = 3) with significant disease, was found at SCA. Moreover, the mean percentage of count density in the males vs females in the inferior wall, extracted from RC-GSPECT and GSPECT, was 69.3 ± 14.7, 65.3 ± 13.0 ($r = 0.76$, $P < .001$) vs 82.2 ± 9.4, 77.3 ± 9.1 ($r = 0.91$, $P < .001$), respectively.

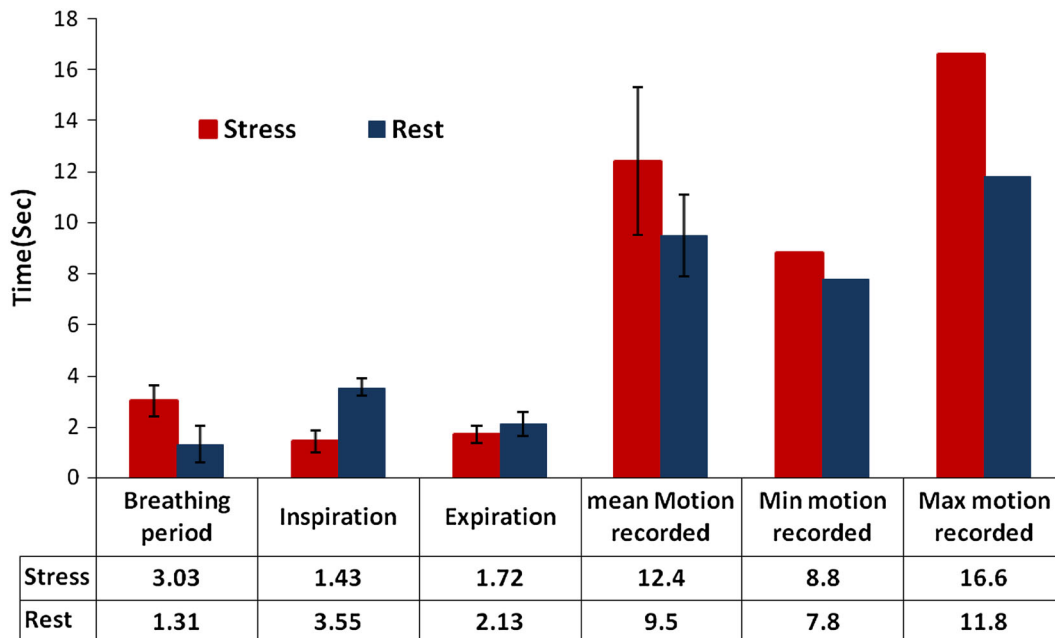In addition, the mean differences of the maximal percentage uptake between the two methods in the



**Figure 6.** Mean and standard deviation of breathing periods and superior-inferior motion of the patient's chest during the stress and rest imaging. Values are expressed as mean ± SD.

**Table 1.** The demographic data

|  | Number of patients | Percentage |
|---|---|---|
| Patients |  |  |
|   Female | 15 | 57.70 |
|   Male | 11 | 42.30 |
| Myocardial perfusion scan | 26 |  |
|   Normal perusion scan | 6 | 26.90 |
|   Abnormal perusion scan | 19 | 73.10 |
|    Female | 9 | 47.40 |
|    Male | 10 | 52.60 |
|   LAD territory | 22 |  |
|   RCA territory | 11 |  |
|   LCX territory | 10 |  |
| Angiography finding | 14 |  |
|   Normal | 3 |  |
|   SVD | 4 |  |
|   2VD | 4 |  |
|   3VD | 3 |  |
|   LAD > 70% stenosis | 3 |  |
|   LAD < 70% stenosis | 4 |  |
|   RCA > 70% stenosis | 3 |  |
|   RCA < 70% stenosis | 5 |  |
|   LCX > 70% stenosis | 7 |  |
|   LCX < 70% stenosis | 0 |  |

*SVD*, Single-vessel disease; *2VD*, two-vessel disease; *3VD*, three-vessel disease.

**Table 2.** Mean and SD of the anterior, anterolateral, inferolateral, inferior, inferoseptal, and antero-septal walls as well as apex uptake percent in GSPECT and RG-SPECT

| LV walls | Patients without SCA | | | Patients with SCA | | |
|---|---|---|---|---|---|---|
|  | GSPECT | RC-GSPECT | *P* | GSPECT | RC-GSPECT | *P* |
| Anterior | 78.7 ± 7.0 | 77.0 ± 7.6 | .431 | 78.1 ± 8.0 | 77.4 ± 7.9 | .529 |
| Anterolateral | 86.4 ± 8.4 | 86.5 ± 7.2 | .866 | 82.4 ± 12.7 | 83.5 ± 11.4 | .218 |
| Inferolateral | 79.5 ± 11.5 | 81.4 ± 8.9 | .150 | 76.0 ± 13.6 | 76.5 ± 14.1 | .528 |
| Inferior | 73.8 ± 13.3 | 78.9 ± 13.1 | .000 | 72.9 ± 10.5 | 80.4 ± 8.5 | .000 |
| Inferoseptal | 73.1 ± 14.8 | 76.3 ± 15.1 | .015 | 75.6 ± 15.3 | 78.8 ± 14.7 | .001 |
| Anteroseptal | 72.4 ± 15.4 | 75.6 ± 13.2 | .028 | 76.6 ± 11.9 | 80.1 ± 11.3 | .000 |
| Apical | 74.4 ± 12.5 | 75.0 ± 17.2 | .803 | 81.2 ± 5.9 | 80.8 ± 7.6 | .798 |

Values are expressed as mean ± SD.
*P*, *P* value.

inferior, anteroseptal, and inferoseptal walls were 9.61%, 3.95%, and 3.91%, respectively, and the mean difference of the percentage uptake in the total walls was 4.26%. In Figure 7, the polar maps using the two different methods, i.e., GSPECT and RC-GSPECT, are presented. In the RC-GSPECT polar maps, an increase in the uptake in the inferior wall and particularly in the inferoseptal and anteroseptal walls is noticeable in comparison with the GSPECT polar maps.

The *t* test revealed a significant difference between the LVEF ($r = 0.94$, $P < .001$), EDV ($r = 0.94$, $P < .001$), ESV ($r = 0.97$, $P < .001$), and SV ($r = 0.88$, $P < .001$) derived with the GSPECT and RC-GSPECT. The mean and SD of the LVEF, EDV,
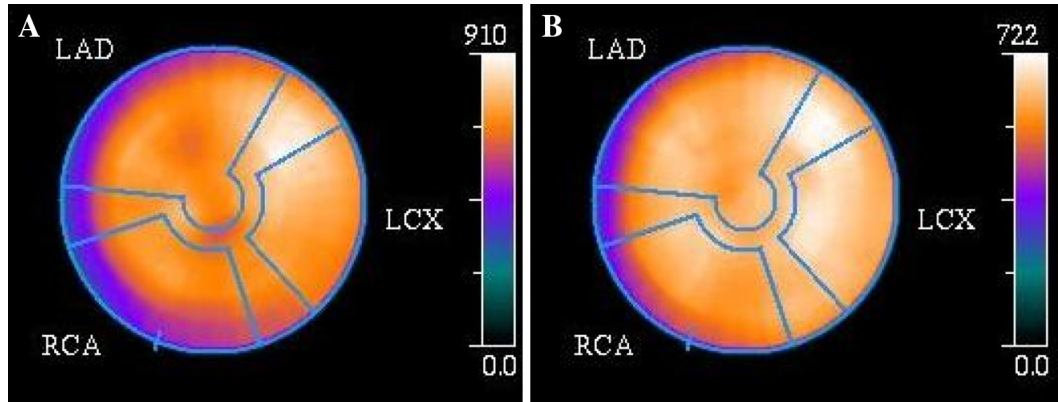
**Figure 7.** GSPECT polar map (*left*) and RG-SPECT polar map (*right*). RG-SPECT polar map shows a higher intensity in the inferior especially in the inferoseptal and anteroseptal walls as compared to the GSPECT polar map.

ESV, and SV-derived with RC-GSPECT and GSPECT are illustrated in Table 3.

In the correlation assessment of the LVEF between GSPECT, RC-SPECT, and echocardiography, better results, i.e., higher correlation, were noted between RC-GSPECT and echocardiography ($r = 0.95$, $P < .001$ vs $r = 0.88$, $P < .001$ for GSPECT) (Figures 8A, 9A). Moreover, the Bland-Altman plots with 95% limit of agreement (Figures 8B, 9B) revealed that the average difference between the echocardiographic LVEFs was lower with the RC-GSPECT (0.08) than with the GSPECT (5.72).

## DISCUSSION

We performed the RC cardiac-gated SPECT imaging in the conventional ECG-gated SPECT acquisition protocol. However, the respiratory gated acquisition requires a sensor that records the respiratory movements. Several methods have been introduced for respiratory motion tracking[12,17,18,20]; the one we used was the RPM system, which has several advantages over the other motion-tracking systems. It has a user-friendly

**Table 3.** Mean and standard deviation of LVEF, EDV, ESV, and SV in GSPECT and RG-SPECT

|           | GSPECT       | RG-SPECT      | r    | P    |
|-----------|--------------|---------------|------|------|
| LVEF (%)  | 53.5 ± 13.4  | 51.5 ± 13.9   | 0.94 | .000 |
| EDV (mL)  | 97.3 ± 31.4  | 101.8 ± 36.6  | 0.94 | .000 |
| ESV (mL)  | 48.3 ± 28.5  | 53.3 ± 34.6   | 0.97 | .000 |
| SV (mL)   | 49.0 ± 13.3  | 48.6 ± 12.7   | 0.88 | .000 |

Values are expressed as mean ± SD.
r, Correlation coefficient; P, P value.

software program compatible with Windows operating system. Moreover, it is not limited by sex, age, and weight, so it is applicable with the majority of patients.

Respiration movement in the axial direction is more significant than that in the lateral direction.[20] The reported range of myocardial motion induced by respiration is 4-18 mm in the cranial-caudal direction.[16] However, the range of breathing motion in our patient population was 7.8-11.8 mm at rest and 8.8-16.6 at stress. This result correlates well with the previous reported values.[21,22]

Data acquisition time was inactive in RC-GSPECT when the cardiac signal was blocked. Hence, acquisition time per projection was 50 seconds in both GSPECT and RC-GSPECT but we first performed GSPECT and then RC-GSPECT acquisition. Total acquisition time of GSPECT was about 14 minutes, and we started RC-GSPECT acquisition immediately after GSPECT acquisition. On the other hand, biokinetic data for tetrofosmin indicates insignificant changes in myocardial distribution up to 180 minutes post-injection.[23] Additionally, $^{99m}$Tc decay is insignificant (<3%) after 14 minutes. Therefore, it can be concluded that the acquisition time difference between RC-GSPECT and GSPECT is unimportant.

Respiratory-related diaphragmatic artifacts are produced during normal breathing with a range of 10-20 mm amplitude. This is clinically relevant that the severity of respiratory artifacts in the same individual varies in different conditions, i.e., stress and rest with deeper and shallower ranges of motion, respectively.[8] Our patients were studied with normal breathing in rest condition and then with pharmacological stress (Dipyridamole). The peak of hemodynamic effects of Dipyridamole has been mentioned to be at approximately the seventh minute after starting infusion and it
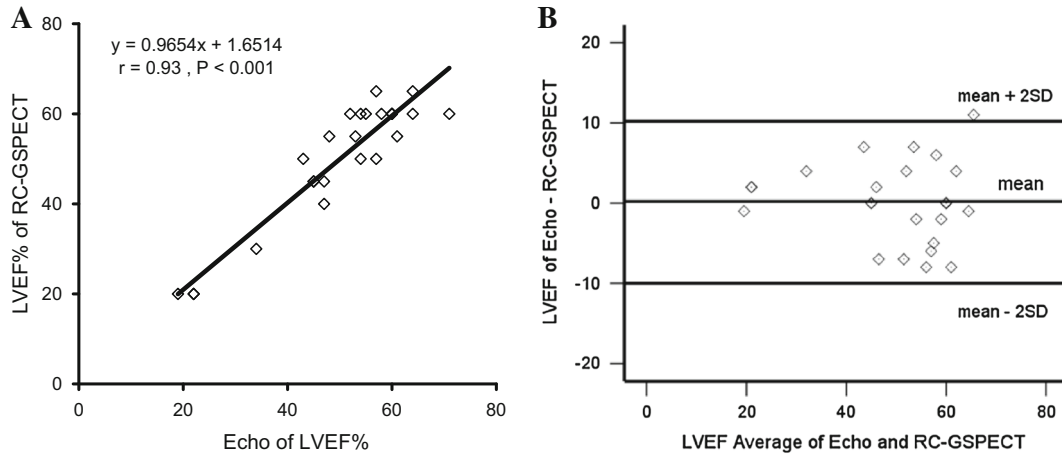
**Figure 8.** Correlation between LVEF of RG-SPECT and echocardiography: linear regression analysis (**A**) and Bland-Altman plot (**B**).
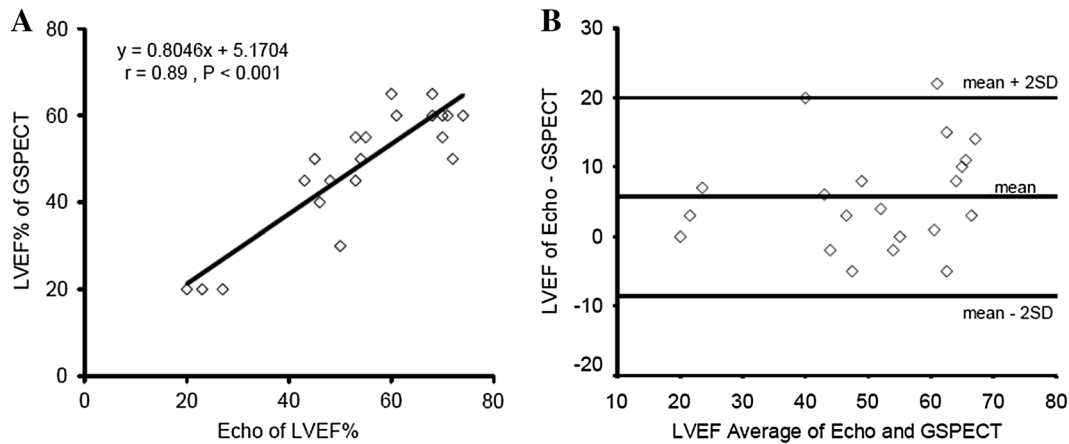


**Figure 9.** Correlation between LVEF of GSPECT and echocardiography: linear regression analysis (**A**) and Bland-Altman plot (**B**).

may last 30-45 minutes after the infusion is completed.[24-26] On the other hand, Dipyridamole is also highly bound to plasma proteins, and the extended-release formulation has a plasma half-life of 13 hours.[27] In view of the fact that shortness of breath and dyspnea are common side effects of Dipyridamole, occurring in some patients,[24-26] we applied RC-GSPECT at both stress and rest acquisitions and compared the results with those of GSPECT in terms of perfusion quantification, and regional and global LV function.

Pitman et al[8] explained the effect of diaphragmatic respiratory motion on the inferior wall as cold artifacts in myocardial SPECT by an anthropomorphic phantom. They introduced and recommended clinical use of respiratory attenuation correction for myocardial SPECT studies to eliminate diaphragmatic motion artifacts. In their clinical studies, when comparing the polar maps of RC-GSPECT and GSPECT, significantly higher

percentage count density was noted in the inferior wall using RC-GSPECT. In another study, Beach et al[17] monitored patient motion by the Polaris motion-tracking system. They clearly showed a significant motion artifact in the anteroseptal and inferior regions of the LV consistent with the axial motion induced by respiration. Bruyant et al[28] performed correction of the respiratory motion of the cardiac images by tracking the center of the mass of threshold projections. Respiratory motion was proved to simulate a lower uptake in the inferior wall of the LV, which could be restored by respiratory motion correction. It is expected that the inferior wall would suffer more from respiratory motion blur than the other walls. In our study, this effect was obvious in all the polar maps as a decrease in count density in the inferior wall, especially in the obese patients.

In clinical studies for lowering the diaphragmatic attenuation in myocardial perfusion imaging (MPI),

prone imaging and attenuation correction (AC) methods have been recommended. The main disadvantage of prone imaging is the need for additional imaging and acquisition time.[29] On the other hand, AC methods for emission tomography require determination of an attenuation map based on transmission scanning by an external radionuclide source or x-ray CT.[30] These methods vary in complexity, accuracy, and computation time required. To date, the most accurate AC techniques are based on measured transmission data acquired before (pre-injection), during (simultaneous), or after (post-injection) the emission scan. The disadvantages of transmission scanning are longer study periods (two separate acquisitions), possibility of inappropriate photon registration between acquisitions due to patient motion, and cross-contamination resulting from scattering between the transmission and emission data.[30] On the other hand, the hybrid SPECT-CT systems are expensive and not widely available and misregistration of the images can occur.[31] Another potential disadvantage of x-ray CT method is that it may contribute to additional patient radiation dose.[31] Moreover, artifacts due to respiration or patient movement, misregistration, and extracardiac radiotracer uptake can be amplified by the iterative algorithms that are employed in AC reconstructions and processing.[30,32] To overcome the difficulties associated with transmission-based AC and the limitations of current attenuation correction, we would propose a feasible and available method, capable of eliminating the respiratory motion effect and—to some extant—diaphragmatic attenuation, especially in obese patients, in MPI studies.

In this investigation, 4D-MSPECT software was used for the quantitative analysis of the LV regional myocardial perfusion and function. 4D-MSPECT exhibits excellent patient-specific reproducibility of quantitative-gated SPECT perfusion data acquired on different imaging systems with slope values near unity for LVEF values.[33]

Comparing the polar maps of the GSPECT and RC-GSPECT, the maximal changes were in the inferior, anteroseptal, and inferoseptal walls with higher count density in RC-GSPECT. Moreover, we evaluated the LV function, EDV, ESV, and SV with both RC-GSPECT and GSPECT (Table 3). Compared to echocardiography, however, a better correlation was found with RC-GSPECT. In fact, RC-GSPECT was performed in the expiration phase, in which a negative pressure is induced in the thorax, causing an increase in EDV and ESV and thus a decrease in LVEF, as we found in our study.

Simulation study was based on the use of the NCAT phantom with variables of cardiac and respiratory motion in MPI. The lower bin compared to the summation of the upper and middle bins as well as the total bin of the respiratory cycle demonstrated that the maximal changes were in the inferior, anteroseptal, and inferoseptal walls with higher count density. Using simulation data, we verified that the RC-GSPECT method could improve the quality of MPI, particularly in the above-mentioned walls.

## LIMITATIONS OF STUDY

A longer total acquisition time could be assumed as one of our limitations, which was 33 minutes (14 and 19 minutes on average for GSPECT and RC-GSPECT, respectively). Nevertheless, total acquisition time in RC-GSPECT was lower than total acquisition time with a single-head gamma camera.

Our method limitation in RC-GSPECT was missing some cardiac cycles during RC. Since the RC-GSPECT may a feasible method for respiratory motion correction in MPI, in the future, we can save all of the cardiac cycles in the next step similar to list mode data acquisition.

Another limitation that could be considered for our study is the width of the acceptance window for gating. There is no clear consensus on the tolerance window for the frame/bin length in gated SPECT acquisitions. On the whole, the narrower the window, the more physiologic the data, but the study may suffer from low count density and/or inappropriate increase in the acquisition length. Classically, it is recommended that cardiac cycles exceeding 30%-40% deviation from the average cycle length should be excluded for the functional information but not for the evaluation of the LV perfusion if the camera rotation is set to a fixed time duration per step.[34] As all the patients with arrhythmia were excluded from our study in the first place, there was no serious limitation to widen the acceptance window for R-R interval up to 80% in order not to lose any acceptable RC cardiac cycles.

## CONCLUSION

We proposed a new approach for respiratory and cardiac-gated SPECT to eliminate respiratory motion artifacts in obese patients, especially in females. Our results indicate that the RC-GSPECT method may improve the quality of Dipyridamole stress and rest MPI, not least in the inferior wall by omitting the adverse effect of respiratory motion on this region. However, further investigation should be undertaken to validate this approach for exercise MPI.

## NEW KNOWLEDGE GAINED

In this study we proposed a new approach for respiratory and cardiac-gated SPECT to eliminate respiratory motion artifacts. RC-GSPECT is a feasible method in MPI studies and may play an important role to improve the quality of MPI images, particularly in the inferior wall. Using simulation data, we verified that the RC-GSPECT method could improve the quality of MPI, particularly in the above-mentioned walls.

## Acknowledgments

## Disclosure

## References

1. Germano G, Erel J, Kiat H, Kavanagh PB, Berman DS. Quantitative LVEF and qualitative regional function from gated thallium-201 perfusion SPECT. J Nucl Med 1997;38:749-54.
2. Go V, Bhatt MR, Hendel RC. The diagnostic and prognostic value of ECG-gated SPECT myocardial perfusion imaging. J Nucl Med 2004;45:912-21.
3. Segars W, Sturgeon G, Mendonca S, Grimes J, Tsui B. 4D XCAT phantom for multimodality imaging research. Med Phys 2010;37:4902-15.
4. Redgate S, Barber DC, Abdallah A-M, Wendy TB. Using a registration-based motion correction algorithm to correct for respiratory motion during myocardial perfusion imaging. Nucl Med Commun 2013;34:787-95.
5. Pretorius PH, King MA, Tsui BM, LaCroix KJ, Xia W. A mathematical model of motion of the heart for use in generating source and attenuation maps for simulating emission imaging. Med Phys 1999;26:2323-32.
6. Reutter BW, Klein GJ, Huesman RH. Automated 3-D segmentation of respiratory-gated PET transmission images. IEEE Trans Nucl Sci 1997;44:2473-6.
7. McClelland J, Hawkes DJ, Schaeffter T, King AP. Respiratory motion models: A review. Med Image Anal 2013;17:19-42.
8. Pitman AG, Kalff V, Van Every B, Risa B, Barnden LR, Kelly MJ. Effect of mechanically simulated diaphragmatic respiratory motion on myocardial SPECT processed with and whitout attenuation correction. J Nucl Med 2002;43:1259-67.
9. Vedam SS, Keall PJ, Kini VR, Mostafavi H, Shukla HP, Mohan R. Acquiring a four-dimensional computed tomography dataset using an external respiratory signal. Phys Med Biol 2003;48:45-62.
10. Fredrickson JO, Wegmuller H, Herfkens RJ, Pelc NJ. Simultaneous temporal resolution of cardiac and respiratory motion in MR imaging. Radiology 1995;195:169-75.
11. Rahmim A, Tang J, Zaidi H. Four-dimensional image reconstruction strategies in cardiac-gated and respiratory-gated PET imaging. PET Clin 2013;8:51-67.
12. Polycarpou I, Tsoumpas C, King AP, Marsden PK. Impact of respiratory motion correction and spatial resolution on lesion detection in PET: A simulation study based on real MR dynamic data. Phys Med Biol 2014;59:697.
13. Pépin A, Daouk J, Bailly P, Hapdey S, Meyer M-E. Management of respiratory motion in PET/computed tomography: The state of the art. Nucl Med Commun 2014;35:113.
14. Darwesh RM, Shin E, Morgan PS, Perkins AC. Improved visualization of perfusion defects by respiratory-gated SPECT: A phantom simulation study. Nucl Med Commun 2014;35:189-96.
15. Sakaguchi K, Hosono M, Otsuka M, Hanaoka K, Usami K, Uto T, et al. Dynamic sequence respiratory gated perfusion pulmonary SPECT without external tracking device. Ann Nucl Med 2013;27:65-73.
16. Kovalski G, Israel O, Keidar Z, Frenkel A, Sachs J, Azhari H. Correction of heart motion due to respiration in clinical myocardial perfusion SPECT scans using respiratory gating. J Nucl Med 2007;48:630-6.
17. Beach RD, Pretorius PH, Boening G, Bruyant P, Feng B, Fulton R, et al. Feasibility of stereo-infrared tracking to monitor patient motion during cardiac SPECT imaging. IEEE Trans Nucl Sci 2004;51:2693-8.
18. Livieratos L, Stegger L, Bloomfield PM, Schafers K, Bailey DL, Camici PG. Rigid body transformation of list-mode projection data for respiratory motion correction in cardiac PET. Phys Med Biol 2005;50:3313-22.
19. Bland JM, Altman DG. Statistical methods for assessing agreement between two methods of clinical measurement. Lancet 1986;8:307-10.
20. Cho K, Kumiata S, Okada S, Kumazaki T. Development of respiratory gated myocardial SPECT system. J Nucl Cardiol 1999;6:20-8.
21. Vedam SS, Kini VR, Keall PJ, Ramakrishnan V, Mostafavi H, Mohan R. Quantifying the predictability of diaphragm motion during respiration with a noninvasive external marker. Med Phys 2003;30:505-13.
22. Nehrke K, Börnert P, Manke D, Böck JC. Free-breathing cardiac MR imaging: Study of implications of respiratory motion-initial results. Radiology 2001;220:810-5.
23. Pillay M, Cox PH, Schönfeld DHW, Mathews S. Tc-99m tetrofosmin myocardial distribution 4 hours post injection. Int J Cardiovasc Imaging 1996;12:127-35.
24. Zaret BL, Beller GA. Clinical nuclear cardiology: State of the art and further directions. 4th ed. Philadelphia: Mosby, Inc.; 2010.
25. Laarman G, Niemeyer MG, Van Der Wall EE, Verzijlbergen FJ, Bruschke AV, Ascoop CA. Dipyridamole thallium testing: Noncardiac side effects, cardiac effects, electrocardiographic changes and hemodynamic changes after dipyridamole infusion with or without exercise. Int J Cardiol 1988;20:231-8.
26. Botvinick EH, Dae MW. Dipyridamole perfusion scintigraphy. Semin Nucl Med 1991;21:242-65.
27. Lenz TL, Hilleman DE. Aggrenox: A fixed-dose combination of aspirin and dipyridamole. Ann Pharmacother 2000;34:1283-90.
28. Bruyant P, King MA, Pretorius PH. Correction of the respiratory motion of the heart by tracking of the center of mass of thresholded projections: A simulation study using the dynamic MCAT phantom. IEEE Trans Nucl Sci 2002;49:2159-66.
29. Slomka PJ, Nishina H, Abidov A, Hayes SW, Friedman JD, Berman DS, et al. Combined quantitative supine-prone myocardial perfusion SPECT improves detection of coronary artery disease and normalcy rates in women. J Nucl Cardiol 2007;14:44-52.
30. Könik A, Kikut J, Lew R, Johnson K, King MA. Comparison of methods of acquiring attenuation maps for cardiac SPECT in the presence of respiratory motion. J Nucl Cardiol 2013;20:1093-107.

31. Goetze S, Brown TL, Lavely WC, Zhang Z, Bengel FM. Attenuation correction in myocardial perfusion SPECT/CT: Effects of misregistration and value of reregistration. J Nucl Med 2007;48:1090-5.

32. Celler A, Dixon KL, Chang Z, Blinder S, Powe J, Harrop R. Problems created in attenuation-corrected SPECT images by artifacts in attenuation maps: A simulation study. J Nucl Med 2005;46:335-43.

33. Nakajima K, Higuchi T, Taki J, Kawano M, Tonami N. Accuracy of ventricular volume and ejection fraction measured by gated myocardial SPECT: Comparison of 4 software programs. J Nucl Med 2001;42:1571-8.

34. Hansen CL, Goldstein RA, Berman DS, Churchwell KB, Cooke D, Corbett JR, et al. Myocardial perfusion and function single photon emission computed tomography. J Nucl Cardiol 2006;13:97-120.